

MSSM Higgs bosons associated with high- p_T jets
at hadron colliders

Oliver Brein ¹ and Wolfgang Hollik ²

*Max-Planck-Institut für Physik,
Föhringer Ring 6, D-80805 München, Germany*

Abstract

The cross section for the production of the lightest neutral Higgs boson in association with a high- p_T hadronic jet, calculated in the framework of the minimal supersymmetric standard model (MSSM), is presented. The expectations for the hadronic cross section at the Large Hadron Collider are discussed using reasonable kinematical cuts. In particular the contributions from superpartner loops to the cross section and their dependence on the parameters of the MSSM are investigated and found to be significant. Comparisons show that the production rate for $h^0 + \text{jet}$ in the MSSM can differ widely from the corresponding standard-model prediction.

¹E-mail: obr@mppmu.mpg.de

²E-mail: hollik@mppmu.mpg.de

1 Introduction

The search for the Higgs boson is a central task at hadron colliders like the Tevatron and the LHC. Most promising Higgs production processes are those with rates high enough for detection and with a clean signal that can be separated effectively from the background processes [1, 2]. Especially, the detection of a Standard Model Higgs boson with a mass roughly between 100 and 140 GeV at the LHC is rather difficult, because the predominant decays of the Higgs bosons into $b\bar{b}$ -pairs are swamped by the large QCD two-jet background [3]. Therefore, only in combination with the rare decay of the Higgs boson into two photons, is the inclusive single Higgs boson production considered the best search channel in this mass range at LHC to date. The theoretical prediction for the inclusive single Higgs production cross section has been studied in great detail for the standard model even including NNLO QCD corrections [4]. Alternatively and in order to fully explore the Higgs detection capabilities of the LHC detectors one can investigate more exclusive channels like e.g. Higgs production in association with a high- p_T hadronic jet. The main advantage of this channel is the richer kinematical structure of the events compared to the inclusive single Higgs production. This allows for refined cuts increasing the signal-to-background ratio.

The process $pp \rightarrow H + \text{jet} + X$ in the standard model (SM) has been studied more than a decade ago by several authors [5, 6, 7] concentrating on different Higgs decay signals like $\tau^+\tau^-$ in [5], W^+W^- and ZZ in [6] and $b\bar{b}$ in [7]. Recently, a detailed signal-to-background analysis of this Higgs boson production process followed by the Higgs decaying into two photons appeared [1, 8] with promising results. But, in the framework of the minimal supersymmetric standard model (MSSM) the theoretical prediction for $pp \rightarrow H + \text{jet} + X$ is incomplete, missing the contribution of the superpartners, like squarks and gluinos, in contrast to the inclusive Higgs production, where the superpartner contributions are even known at two-loop accuracy in the heavy squark limit [9].

In this paper we present a complete one-loop result in the MSSM for the production of a neutral Higgs boson in association with a high- p_T hadronic jet ($pp \rightarrow h^0 + \text{jet} + X$). Furthermore, we explore the contribution of the previously unknown superpartner loops to the cross section numerically for the three benchmark scenarios for the MSSM Higgs search at LEP [11] within regions not yet excluded by experimental constraints. The so-called large- μ scenario is suitably modified to yield Higgs masses not excluded by LEP Higgs searches. We also compare the MSSM result to leading order with the SM result to the same order. The numerical analyses are done for LHC energies and parton luminosities.

2 Partonic Processes

There are three partonic processes contributing to the hadronic Higgs-plus-jet signal process: the production of a Higgs boson and a gluon by gluon fusion or quark-antiquark annihilation ($gg, q\bar{q} \rightarrow gh^0$), and of a Higgs boson accompanied by a quark via quark-gluon scattering ($qg \rightarrow qh^0, \bar{q}g \rightarrow \bar{q}h^0$). Our analysis considers all three processes, although only

gluon fusion and quark-gluon scattering lead to significant rates at the LHC.

2.1 Gluon fusion ($gg \rightarrow gh^0$)

In our conventions, $gk_{1,2,3}$, p denote the momenta $\sigma_{1,2,3}$ the helicities, and a, b, c the colour indices of the particles in the process

$$g(k_1, a, \sigma_1) + g(k_2, b, \sigma_2) \rightarrow g(k_3, c, \sigma_3) + h^0(p).$$

We make use of the partonic kinematical invariants

$$\hat{s} = (k_1 + k_2)^2, \quad \hat{t} = (k_1 - k_3)^2, \quad \hat{u} = (k_1 - p)^2, \quad (1)$$

obeying the relation

$$\hat{s} + \hat{t} + \hat{u} = m_{h^0}^2. \quad (2)$$

After averaging and summing over the spin and colour degrees of freedom of the incoming and outgoing particles, respectively, the differential cross section reads

$$\frac{d\sigma_{gg \rightarrow gh^0}}{d\hat{t}} = \frac{1}{16\pi\hat{s}^2} \frac{1}{4} \sum_{\sigma_1, \sigma_2, \sigma_3 = \pm 1} \frac{1}{64} \sum_{a, b, c = 1}^8 |\mathcal{M}_{\sigma_1 \sigma_2 \sigma_3}^{abc}|^2, \quad (3)$$

containing the helicity amplitudes

$$\mathcal{M}_{\sigma_1 \sigma_2 \sigma_3}^{abc} = \varepsilon_{\sigma_1}^\mu(k_1) \varepsilon_{\sigma_2}^\nu(k_2) \varepsilon_{\sigma_3}^{*\rho}(k_3) \widetilde{\mathcal{M}}_{\mu\nu\rho}^{abc}, \quad (4)$$

where $\varepsilon_{\sigma_1}^\mu(k_1)$, $\varepsilon_{\sigma_2}^\nu(k_2)$ and $\varepsilon_{\sigma_3}^{*\rho}(k_3)$ are the polarisation vectors of the gluons. As a general feature of the amplitude, the transversality of gluons gives useful identities

$$k_1^\mu \varepsilon_{\sigma_2}^\nu(k_2) \varepsilon_{\sigma_3}^{*\rho}(k_3) \widetilde{\mathcal{M}}_{\mu\nu\rho}^{abc} = \varepsilon_{\sigma_1}^\mu(k_1) k_2^\nu \varepsilon_{\sigma_3}^{*\rho}(k_3) \widetilde{\mathcal{M}}_{\mu\nu\rho}^{abc} = \varepsilon_{\sigma_1}^\mu(k_1) \varepsilon_{\sigma_2}^\nu(k_2) k_3^\rho \widetilde{\mathcal{M}}_{\mu\nu\rho}^{abc} = 0, \quad (5)$$

which allow cross-checks of our one-loop calculation of $\widetilde{\mathcal{M}}_{\mu\nu\rho}^{abc}$.

The process $gg \rightarrow gh^0$ is a pure quantum effect, induced at the one-loop level. The one-loop Feynman graphs contributing to the process divide in those which contain a closed quark loop (Figure 1) and those which contain a closed loop of virtual squarks (Figure 2). The quark-loop graphs contain either the loop-induced Higgs-gluon-gluon coupling with one of the gluons exchanged internally, or a box-type topology. For the squark loop amplitudes the same subdivision applies, if the fact is taken into account that certain $(n-1)$ -point loop graphs are connected to certain n -point loop graphs due to the scalar nature of the squarks. The connection is that certain triangle loop graphs can be obtained from certain box loop graphs by shrinking one squark line to a point. The Feynman graphs for the corresponding Standard Model process are analogous to the set of quark loop graphs.

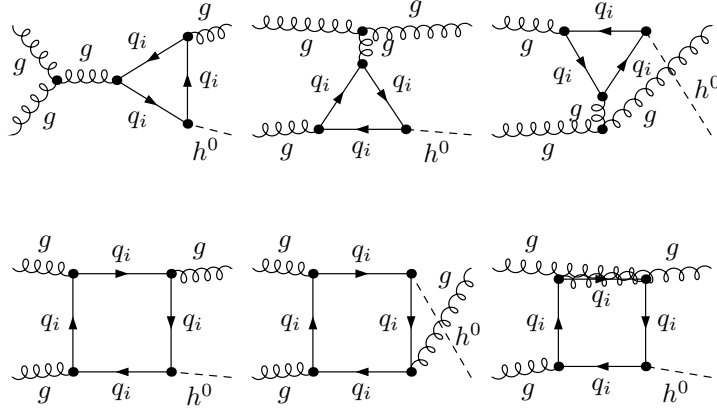


Figure 1: Quark loop graphs for the process $gg \rightarrow gh^0$ in leading order. Feynman graphs with opposite direction of charge flow are not depicted.

2.2 Quark-gluon scattering ($qg \rightarrow qh^0$, $\bar{q}g \rightarrow \bar{q}h^0$)

With the same conventions for momenta and helicities as before, we consider the processes

$$\begin{aligned} g(k_1, a, \sigma_1) + q(k_2, i, \sigma_2) &\rightarrow q(k_3, j, \sigma_3) + h^0(p) , \\ g(k_1, a, \sigma_1) + \bar{q}(k_2, i, \sigma_2) &\rightarrow \bar{q}(k_3, j, \sigma_3) + h^0(p) . \end{aligned}$$

The labels a and $\sigma_1 (= \pm 1)$ denote the degrees of freedom of colour and helicity of the gluon. a, i, j are the colour indices of the gluon and the (anti-)quark. The Mandelstam variables are defined as in eq. (1) and fulfil the relation (2) in the limit of vanishing quark masses.

The differential cross section for quark scattering averaged over initial and summed over final state colour and helicity d.o.f. is given by

$$\frac{d\sigma_{qg \rightarrow qh^0}}{d\hat{t}} = \frac{1}{16\pi\hat{s}^2} \frac{1}{2} \sum_{\sigma_1=\pm 1} \frac{1}{2} \sum_{\sigma_2, \sigma_3=\pm\frac{1}{2}} \frac{1}{8} \sum_{a=1}^8 \frac{1}{3} \sum_{i,j=1}^3 |\mathcal{M}_{\sigma_1\sigma_2\sigma_3}^{aj}|^2 , \quad (6)$$

containing the helicity amplitudes

$$\mathcal{M}_{\sigma_1\sigma_2\sigma_3}^{aj} = \varepsilon_{\sigma_1}^\mu(k_1) \widetilde{\mathcal{M}}_{\mu\sigma_2\sigma_3}^{aj} , \quad (7)$$

and likewise for anti-quarks. The polarisation vector of the incoming gluon is denoted by $\varepsilon_{\sigma_1}^\mu(k_1)$. The transversality of the helicity amplitudes (c.f. section 2.1) is expressed by the identity,

$$k_1^\mu \widetilde{\mathcal{M}}_{\mu\sigma_2\sigma_3}^{aj} = 0 \quad (8)$$

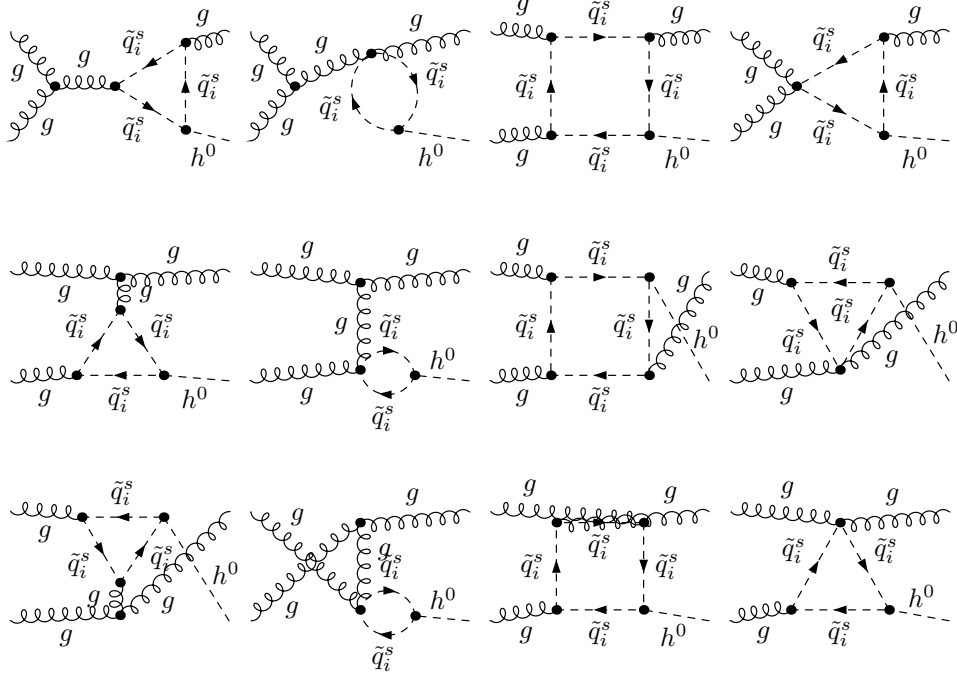


Figure 2: Scalar quark loop graphs for the process $gg \rightarrow gh^0$ in leading order. Feynman graphs with opposite direction of charge flow are not depicted.

which has been used as a check of our results .

The Yukawa couplings of the Higgs boson h^0 to the light quarks ($q = u, d, s, c$) are negligible. Hence, the leading order amplitude for $qg \rightarrow qh^0$ is loop-induced, described by the Feynman graphs of $\mathcal{O}(g_S^3 g_2)$ depicted in Figure 3.³ The Feynman graphs divide into those with a closed quark (q_i) loop of triangle-type and those with a loop of virtual superpartners (squarks, \tilde{q}_i^s , and gluinos, \tilde{g}) of triangle- and of box-type. There are also electroweak contributions $\propto g_S g_2^3$ at the one-loop level. We calculated those contributions and found their effect on the numerical results for the partonic cross section to be at most 2 - 3 % of the QCD contribution. They will be neglected in the following.

For the b -quark, the Yukawa-coupling to the Higgs boson cannot be neglected, especially for large values of $\tan \beta$, and leads to a tree-level contribution, as displayed in Figure 4.

The Feynman graphs appearing in the corresponding Standard Model process are analogous to the set of quark loop graphs in Figure 3. Thus, in the MSSM there appear additional Feynman-graph topologies which are not present in the Standard Model and which may even change the angular distribution of the final-state particles compared to the Standard Model expectation.

³ g_S and g_2 are the coupling constants of the strong and weak interaction respectively.

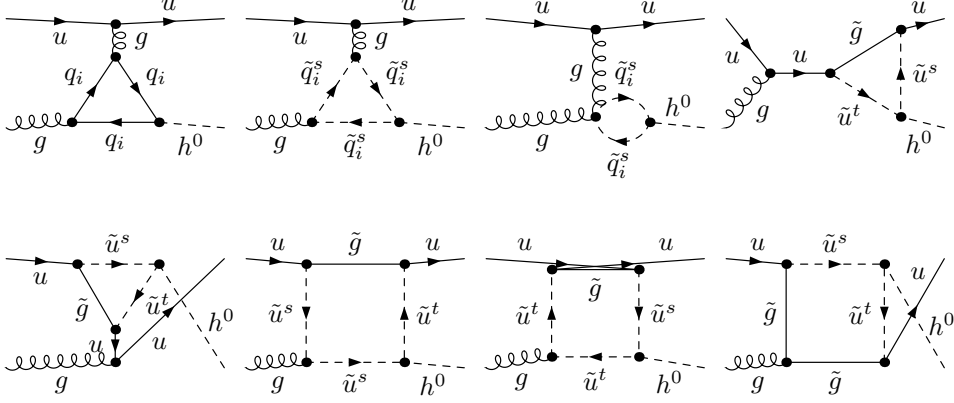


Figure 3: Loop graphs for the process $ug \rightarrow uh^0$ in leading order. Feynman graphs with opposite direction of charge flow are not depicted. For the scattering of the other quarks (d, c, s) the graphs look similar.

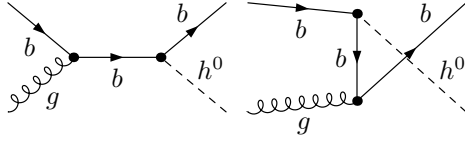


Figure 4: Feynman graphs for the b -quark processes in leading order. The graphs represent the amplitude for the process $bg \rightarrow bh^0$ if the time axis points to the right and $b\bar{b} \rightarrow gh^0$ if it points from up to down.

2.3 Quark-antiquark annihilation ($q\bar{q} \rightarrow gh^0$)

With the same notations for momenta, helicities and colour as above, the parton reaction

$$q(k_1, i, \sigma_1) + \bar{q}(k_2, j, \sigma_2) \rightarrow g(k_3, a, \sigma_3) + h^0(p), \quad (9)$$

has the differential cross section

$$\frac{d\sigma_{q\bar{q} \rightarrow gh^0}}{d\hat{t}} = \frac{1}{16\pi\hat{s}^2} \frac{1}{4} \sum_{\sigma_1, \sigma_2 = \pm\frac{1}{2}} \frac{1}{9} \sum_{i, j=1}^3 \sum_{\sigma_3 = \pm 1} \sum_{a=1}^8 |\mathcal{M}_{\sigma_1\sigma_2\sigma_3}^{aij}|^2, \quad (10)$$

containing the helicity amplitudes

$$\mathcal{M}_{\sigma_1\sigma_2\sigma_3}^{aij} = \varepsilon_{\sigma_3}^{*\mu}(k_3) \widetilde{\mathcal{M}}_{\mu\sigma_1\sigma_2}^{aij} \quad (11)$$

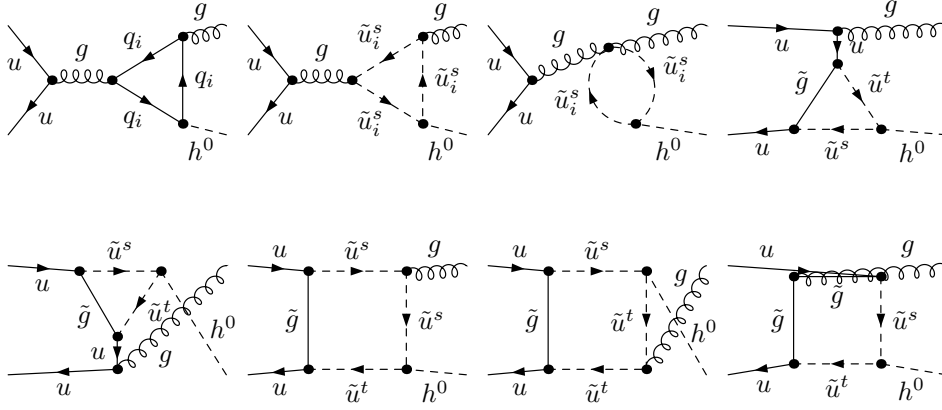


Figure 5: Feynman graphs for the process $u\bar{u} \rightarrow gh^0$ in leading order. Feynman graphs with opposite direction of charge flow are not depicted. For the scattering of the other quarks (d, c, s) the Feynman graphs look similar.

with the polarisation vector $\varepsilon_{\sigma_3}^{*\mu}(k_3)$ of the outgoing gluon. Analogously to the transversality check of the helicity amplitudes in the previous two sections, we verified that the helicity amplitudes vanish if the polarisation vector of the gluon is replaced by its momentum.

Again, since the Yukawa-couplings of the light quarks to the Higgs boson can be neglected, the amplitudes for $q\bar{q} \rightarrow gh^0$ ($q = u, d, s, c$) are loop-induced. The Feynman graphs contributing to these amplitudes divide into the ones of Standard Model type, which contain a quark loop, and the others with virtual superpartners, squarks and gluinos (see Figure 5). As in b -quark–gluon scattering, the b Yukawa coupling to the Higgs boson cannot be neglected, yielding tree-level graphs obtained by crossing those of Figure 4.

The calculations of the partonic cross sections have been performed with the help of the computer programs FeynArts and FormCalc [20].

3 Hadronic Cross Section

The hadronic cross section for $h^0 + \text{jet}$ production with a total hadronic CMS energy \sqrt{S} can be written as a convolution [17]

$$\begin{aligned} \sigma(AB \rightarrow h^0 + \text{jet} + X) = & \int_{\tau_0}^1 d\tau \left(\frac{d\mathcal{L}_{gg}^{AB}}{d\tau} \sigma_{gg \rightarrow gh^0}(\tau S, \alpha_S(\mu_R)) \right. \\ & \left. + \sum_{q=u,\bar{u},\dots,b,\bar{b}} \frac{d\mathcal{L}_{q\bar{q}}^{AB}}{d\tau} \sigma_{q\bar{q} \rightarrow qh^0}(\tau S, \alpha_S(\mu_R)) + \sum_{q=u,\dots,b} \frac{d\mathcal{L}_{q\bar{q}}^{AB}}{d\tau} \sigma_{q\bar{q} \rightarrow gh^0}(\tau S, \alpha_S(\mu_R)) \right) \quad (12) \end{aligned}$$

with the parton luminosity

$$\frac{d\mathcal{L}_{nm}^{AB}}{d\tau} = \int_{\tau}^1 \frac{dx}{x} \frac{1}{1 + \delta_{nm}} \left[f_{n/A}(x, \mu_F) f_{m/B}\left(\frac{\tau}{x}, \mu_F\right) + f_{m/A}(x, \mu_F) f_{n/B}\left(\frac{\tau}{x}, \mu_F\right) \right], \quad (13)$$

where $f_{n/A}(x, \mu_F)$ denotes the density of partons of type n in the hadron A carrying a fraction x of the hadron momentum at the scale μ_F and $(A, B) = (p, p)$ for the LHC [and (p, \bar{p}) for the Tevatron]. The lower bound of the τ -integration (τ_0) determines the minimal invariant mass of the parton system, $\hat{s}_0 = \tau_0 S$. In our case, τ_0 depends on the kinematical cuts applied in order to have high- p_T jets not too close to the beam-pipe.

The angular dependences of the differential cross sections in the CMS of the processes $gg \rightarrow gh^0$ and $qg \rightarrow qh^0$ (with $m_q = 0$) diverge in the collinear limit, i.e. for scattering angle $\hat{\theta} = 0$, or $\hat{t} = 0$. In the gluon fusion process the final state gluon can be collinear to either of the incoming gluons. Therefore, the gluon fusion cross section also diverges for $\hat{\theta} = \pi$, or $\hat{u} = 0$. These regions of phase space, however, are excluded when we require a high- p_T jet originating from the final-state parton. Specifically, if we impose the condition $k_{3,T} > p_{T,\min}$ for the transverse momentum of the outgoing parton $k_{3,T}$, one obtains an energy and an angular cut,

$$\sqrt{\hat{s}} > p_{T,\min} + \sqrt{m_h^2 + p_{T,\min}^2} \equiv \sqrt{\tau_0 S}, \quad (14)$$

$$|\cos \hat{\theta}| < \sqrt{1 - \frac{4 \hat{s} p_{T,\min}^2}{(\hat{s} - m_h^2)^2}}. \quad (15)$$

On top, in order to avoid high- p_T partons with very small angles to the beam axis in the laboratory frame, $\hat{\theta}_{\text{lab}}$, we impose a cut on the pseudo-rapidity of the outgoing parton $\eta_{3,\text{lab}}$ ($\equiv -\ln \tan(\hat{\theta}_{\text{lab}}/2)$) in the laboratory frame, $|\eta_{3,\text{lab}}| < \eta_{\max}$, thus constraining the scattering angle in the laboratory according to

$$2 \arctan e^{-\eta_{\max}} < \hat{\theta}_{\text{lab}} < 2 \arctan e^{\eta_{\max}}. \quad (16)$$

This requirement leads to bounds on $\hat{\theta}$, or \hat{t} , respectively in the CMS frame. All integrated partonic cross sections

$$\sigma_{nm \rightarrow m'h^0}(\hat{s}, \alpha_S(\mu_R)) = \int_{\hat{t}_{\min}}^{\hat{t}_{\max}} d\hat{t} \frac{d\sigma_{nm \rightarrow m'h^0}}{d\hat{t}} \quad (n, m, m' \in \{q, g\}) \quad (17)$$

are then evaluated by numerical integration over the \hat{t} -range respecting the cuts $k_{3,T} > p_{T,\min}$ and $|\eta_{3,\text{lab}}| < \eta_{\max}$.

The numerical evaluation has been carried out with the MRST gluon distribution functions [19] and with the renormalisation and factorisation scale μ_R and μ_F chosen both equal to $\sqrt{\hat{s}}$.

4 Numerical Results

In the following discussion we want to illustrate the the MSSM predictions for the hadronic process $pp \rightarrow h^0 + \text{jet} + X$ and outline differences between the cases of MSSM Higgs boson h^0 and of a standard Higgs particle with the same mass. In particular we discuss the influence of the diagrams with the superpartners squarks and gluinos. The cuts chosen for the numerical evaluation are chosen as $p_{T,\text{min}} = 30 \text{ GeV}$ and $\eta_{\text{max}} = 4.5$, which have been used in previous studies in the Standard Model [8].

4.1 Parameters

We adopt for our discussion the three MSSM benchmark scenarios for the Higgs search at LEP, which were originally proposed in [11]. One of them, the large- μ scenario, had to be modified in order to obey the exclusion limit for the Higgs mass set by the latest LEP data [15]. In our discussion we vary the common sfermion mass scale M_{SUSY} . Therefore, brief specifications of the three scenarios with variable sfermion mass scale are given here.

no-mixing scenario : The off-diagonal term $X_t (= A_t - \mu \cot \beta)$ in the top-squark mass matrix is zero, corresponding to a local minimum of m_h as a function of X_t . The supersymmetric Higgsino mass parameter μ is set to -200 GeV , the gaugino mass parameter to $M_2 = 200 \text{ GeV}$, and the gluino mass to $M_{\tilde{g}} = 800 \text{ GeV}$. When $\tan \beta$ is changed, A_t is changed accordingly to insure $X_t = 0$. The settings of the other soft-breaking scalar-quark Higgs couplings are $A_b = A_t$ and $A_q = 0$ ($q = u, d, c, s$).

maximal- m_h scenario : X_t is set to $2M_{\text{SUSY}}$ which yields the maximal value of m_h with respect to stop mixing effects⁴. The other parameters are chosen as in the previous scenario.

large- μ scenario : The key feature of this scenario is a relatively large value of μ ($= 1000 \text{ GeV}$) which leads to strong radiative corrections of the b -quark Yukawa coupling to the Higgs boson. In modification of the original scenario (where $X_t = -300 \text{ GeV}$) we set $X_t = -900 \text{ GeV}$ which gives a maximal Higgs mass of approximately 124 GeV compared to 107 GeV of the original scenario. The other parameters are: $A_b = 0$, $M_2 = 200 \text{ GeV}$ and $M_{\tilde{g}} = 400 \text{ GeV}$.

In order to demonstrate squark effects, we take a common sfermion mass scale M_{SUSY} in all the figures, with a moderately high value of 400 GeV . The mass of the CP-odd Higgs m_A , the ratio of Higgs vacuum expectation values $\tan \beta = v_2/v_1$, and the common sfermion mass scale M_{SUSY} are varied within bounds from direct Higgs and squark searches (c.f. [16]). Additionally, in all scenarios, mixing in the squark sector respects the bounds on additional non-SM contributions to the electroweak ρ -parameter [14]. For the electroweak parameters we use the values given in [16], and for the strong coupling constant $\alpha_S(\mu_R)$, we use the formula including the two-loop QCD corrections for $n_f = 5$ with $\Lambda_{\text{QCD}}^5 = 170$

⁴The choice of X_t applies to the Feynman diagrammatic calculation of m_h [13].

Scenario	no mixing		m_h^{\max}		large μ	
	$(m_A = 400 \text{ GeV})$		$(m_A = 400 \text{ GeV})$		$(m_A = 400 \text{ GeV})$	
$\tan \beta$	6	30	6	30	6	30
$M_{\text{SUSY}} [\text{GeV}]$	400	400	400	400	400	400
$m_h [\text{GeV}]$	100.2	104.5	120.2	123.9	121.0	123.3
$\sigma_{\text{all}}^{\text{MSSM}}$ ($\sigma_{\text{all, no SP}}^{\text{MSSM}}$)	7.50 (6.49)	6.96 (6.10)	3.89 (5.04)	3.65 (4.84)	2.12 (4.89)	1.51 (4.78)
$\sigma_{(gg \rightarrow hg)}^{\text{MSSM}}$	4.81	4.44	2.46	2.31	1.38	0.97
$\sigma_{(qq \rightarrow hg, q=u, \bar{u}, d, \bar{d}, c, \bar{c}, s, \bar{s})}^{\text{MSSM}}$	2.32	2.19	1.17	1.11	0.65	0.46
$\sigma_{(qq \rightarrow hg, q=b, \bar{b})}^{\text{MSSM}}$	0.29	0.26	0.20	0.18	0.07	0.06
$\sigma_{(b\bar{b} \rightarrow hg)}^{\text{MSSM}}$	0.08	0.07	0.06	0.05	0.02	0.02
$\sigma_{(q\bar{q} \rightarrow hg, q=u, d, c, s)}^{\text{MSSM}}$	0.03	0.03	0.02	0.02	0.01	0.01
$\sigma_{\text{all}}^{\text{SM}}$	6.27	5.92	5.07	4.85	4.88	4.75
$\sigma_{(gg \rightarrow Hg)}^{\text{SM}}$	4.07	3.83	3.35	3.20	3.32	3.22
$\sigma_{(qq \rightarrow Hg, q=u, \bar{u}, d, \bar{d}, c, \bar{c}, s, \bar{s})}^{\text{SM}}$	1.86	1.77	1.49	1.43	1.46	1.43
$\sigma_{(qq \rightarrow Hg, q=b, \bar{b})}^{\text{SM}}$	0.23	0.21	0.15	0.14	0.05	0.05
$\sigma_{(b\bar{b} \rightarrow Hg)}^{\text{SM}}$	0.08	0.08	0.06	0.05	0.02	0.02
$\sigma_{(q\bar{q} \rightarrow Hg, q=u, d, c, s)}^{\text{SM}}$	0.03	0.03	0.03	0.03	0.03	0.03

Table 1: MSSM and SM predictions for the hadronic cross section, divided in the contributions from different partonic processes.

MeV which can be found also in [16]. Effects of non-zero widths of the quarks and squarks in the loops are not taken into account because their widths are considerably smaller than their masses and are expected to change the results only little ⁵.

4.2 Discussion

The Higgs-boson couplings to quarks and squarks consist entirely of terms weighted by either $\sin \alpha$ or $\cos \alpha$ (see Appendix A), with α being the mixing angle between the neutral CP-even Higgs fields. Thus, the cross section's dependence on m_A and $\tan \beta$ can be easily inferred from the dependence of α on those parameters and the simple $\tan \beta$ -dependence of the Higgs couplings to quarks and squarks (see eqs. (19) – (23)). To evaluate the Higgs mass m_h and mixing angle α we use the results of the two-loop Feynman diagrammatic calculation in the effective-mixing-angle approximation [13], where the effective mixing

⁵A study of non-zero width effects for a similar process is documented in [10].

angle α is given by

$$\tan \alpha = \frac{-(m_A^2 + m_Z^2) \sin \beta \cos \beta - \hat{\Sigma}_{\phi_1 \phi_2}(0)}{m_Z^2 \cos^2 \beta + m_A^2 \sin^2 \beta - \hat{\Sigma}_{\phi_1}(0) - m_h^2}. \quad (18)$$

Figures 6(a)–(f) and 7(a)–(f) show the results for the hadronic cross section as functions of m_A and $\tan \beta$ for exemplary values of $\tan \beta$ (6 and 30) and m_A (100 and 400 GeV) respectively. In all plots several contributions to the cross section are displayed separately.

Especially for large $\tan \beta$, the b -quark Yukawa coupling is enhanced, and the partonic processes $b(\bar{b})g \rightarrow h^0 b(\bar{b})$ and $b\bar{b} \rightarrow h^0 g$ are dominated by the tree-level amplitude of Figure 4. These tree-level processes are included via the b -quark distribution in the proton, using a running b -quark mass in the Yukawa coupling, which is known to take into account the most important effect of the NLO corrections [18]. The thick solid lines in Figures 6(a)–(f) and 7(a)–(f) show the complete cross section in the MSSM, based on the partonic processes gluon fusion, quark–gluon scattering, and quark–anti-quark annihilation including the b -quark tree-processes. In order to visualize the size of the b -quark effects, we neglect the b -quark distribution in the proton and use only the effectively loop-induced processes for the light quarks ($u, \bar{u}, d, \bar{d}, c, \bar{c}, s, \bar{s}$), as illustrated in Figure 3. The cross section for this case is displayed by the thick dashed lines in Figures 6(a)–(f) and 7(a)–(f).

In order to demonstrate the influence of the virtual superpartners on the result the thin solid and dashed lines show the hadronic cross section obtained by neglecting all diagrams with virtual superpartners in the calculation of the corresponding partonic processes.

Next we discuss the behaviour of the cross section in the three benchmark scenarios.

No-mixing scenario

The behaviour of the hadronic cross section in the no-mixing scenario can be inferred from Figures 6(a) and 6(b), which show the m_A -dependence for $\tan \beta = 6$ and $\tan \beta = 30$ and from Figures 7(a) and 7(b), which show the $\tan \beta$ -dependence for $m_A = 100$ GeV and $m_A = 400$ GeV.

In this scenario the masses of the squarks are essentially independent of the parameters of the MSSM Higgs sector. This is because the $\tan \beta$ -dependent mixing of squarks is either zero by definition (in the scalar top sector) or very small (for all other squarks) and m_A does not enter the squark sector at all in leading order. Therefore, the variation of the cross section with m_A and $\tan \beta$ is determined by the variation of the mass and the couplings of h^0 . For small m_A (< 150 GeV) and especially for large $\tan \beta$, the b -quark Yukawa coupling is strongly enhanced compared to the top-Higgs coupling (see eqs. (19),(22) and (23)). Thus, in this parameter range the b -quark processes dominate the hadronic cross section, and also the loop-induced processes are dominated by the b -quark loops. At large m_A (> 200 GeV) the coupling of the b -Higgs coupling is much smaller than the top-Higgs coupling and therefore the loop-induced processes, mainly the top-quark loops, dominate the hadronic cross section. In this parameter range the superpartners contribute about 15% of the complete result (see Table 1). For large m_A the flat behaviour of the cross

section in Figure 7(b) illustrates, that relevant contributions only come from loops with virtual up-type quarks and squarks, which couple $\propto 1/\sin\beta$ to the h^0 , while down-type quarks and squarks couple $\propto 1/\cos\beta$ (see eqs. (19) – (21)).

Figure 8(a) shows the dependence of the cross section on the sfermion-mass scale M_{SUSY} for $m_A = 200$ GeV and $\tan\beta = 6$. The relative difference between the full result and the one without superpartner loops stays above 10% for M_{SUSY} below 500 GeV.

Maximal- m_h scenario

The m_A -dependence of the hadronic cross section in the maximal- m_h scenario is shown in Figures 6(c) ($\tan\beta = 6$) and 6(d) ($\tan\beta = 30$), and the $\tan\beta$ -dependence in Figures 7(c) ($m_A = 100$ GeV) and 7(d) ($m_A = 400$ GeV).

This scenario is rather similar to the no-mixing scenario as far as the variation of the cross section with m_A and $\tan\beta$ is concerned. The m_A - and $\tan\beta$ -dependences arise almost entirely through the dependence of h^0 mass and couplings, while the squark masses are essentially constant. But there is one crucial difference: the sign of the leading squark-loop contributions is opposite to the no-mixing case, which results in a suppression of the full result instead of an enhancement. This is because the \tilde{t} mixing angle $\theta_{\tilde{t}}$ is approximately $\pi/4$ in the maximal- m_h scenario. Therefore, the leading behaviour of the squark-loop amplitude is governed by the terms proportional to $m_t A_t \cos\alpha/\sin\beta$ in the coupling of the h^0 to the lighter top squark (see eq. (20)). This yields a destructive interference with the quark loops. For $m_A = 400$ GeV, and almost independent of $\tan\beta$, the full result is reduced by about 24% compared to the result with quark loops only (see Table 1).

Figure 8(a) shows the dependence of the cross section on the sfermion mass scale M_{SUSY} for $m_A = 200$ GeV and $\tan\beta = 6$.

Large- μ scenario

The m_A -dependence of the hadronic cross section in the large- μ scenario is shown in Figures 6(e) ($\tan\beta = 6$) and 6(f) ($\tan\beta = 30$) and the $\tan\beta$ -dependence in Figures 7(e) ($m_A = 100$ GeV) and 7(f) ($m_A = 400$ GeV).

The large- μ scenario shows the most pronounced superpartner contribution. The superpartner loops interfere destructively with the quark loops, except when $\tan\beta$ is large and m_A is small simultaneously. In the large- μ scenario, mixing in the \tilde{b} sector increases with $\tan\beta$, resulting in large mixing ($\theta_{\tilde{b}} \approx 45^\circ$) for $\tan\beta \geq 30$. Therefore, for large $\tan\beta$, the terms proportional to $m_b \mu \sin 2\theta_{\tilde{b}}$ in the \tilde{b} -Higgs couplings are dominant, followed by the terms proportional to $m_t A_t \sin 2\theta_{\tilde{t}}$ in the \tilde{t} -Higgs couplings (see eqs. (20) to (23)).

For large m_A the decrease of the cross section lies between 50% and 70% (see Table 1). Figure 8(b) shows the dependence of the cross section on the sfermion-mass scale M_{SUSY} for $m_A = 200$ GeV and $\tan\beta = 6$. The large negative interference between quark and superpartner loops vanishes rapidly with rising M_{SUSY} . Unlike for the other two scenarios the superpartner contribution is already negligible for $M_{\text{SUSY}} > 600$ GeV.

Comparison with the Standard Model

The thin dot-dashed line in Figures 6(a)–(f) and 7(a)–(f) indicates the hadronic cross section in the Standard Model with the mass of the Standard-Model Higgs boson chosen equal to m_h in the MSSM. In this way, we can discuss the difference between the two predictions as a function of the MSSM parameters. Figures 6(a)–(f) show the decoupling behaviour in the MSSM Higgs sector with rising m_A . The MSSM prediction where virtual superpartners are neglected in the calculation (thin solid lines), which corresponds essentially to the case of decoupling superpartners, approaches the SM prediction closely with rising m_A . In this regime h^0 behaves like the Standard Model Higgs boson. However, the full MSSM prediction (thick solid lines) shows a rather large departure from the Standard Model prediction for lower sfermion masses, as in the MSSM parameter scenarios we chose.

In Figure 9 we display the relative difference between the MSSM and the SM prediction of the hadronic cross section plotted versus m_A and $\tan\beta$. The parameters of the maximal- m_h scenario with $M_{\text{SUSY}} = 400$ GeV are chosen as an example. For this moderate value of M_{SUSY} the MSSM prediction for the hadronic cross section is more than 20% below the SM result in the whole area of the m_A - $\tan\beta$ plane displayed.

5 Conclusions

The production of a neutral Higgs boson accompanied by a high- p_T jet is considered advantageous for Higgs boson detection even though the rate is lower than for totally inclusive single Higgs boson production. Refined cuts allow to increase the signal-to-background ratio compared to the inclusive production. We calculate the hadronic cross section for Higgs-plus-jet production with the full set of MSSM Feynman graphs at leading-order QCD. We find a quite substantial cross section ranging from about 0.3 pb to 300 pb depending on the MSSM parameter scenario. Thus, this process might be detectable at the LHC even if the $\gamma\gamma$ -decay channel of the Higgs is considered (see e.g. [1, 8]). The contribution from superpartner loops to the cross section and its dependence on the parameters of the MSSM turns out to be significant. We provide a FORTRAN code for general use.

Acknowledgement.

We thank Georg Weiglein for bringing this topic to our attention. This work was supported in part by the European Community's Human Potential Programme under contract HPRN-CT-2000-00149 "Physics at Colliders".

Appendix

A Higgs couplings

$$g_s[h^0 tt] = -g_2 \frac{m_t}{2m_W} \frac{\cos \alpha}{\sin \beta}, \quad g_s[h^0 bb] = +g_2 \frac{m_b}{2m_W} \frac{\sin \alpha}{\cos \beta}. \quad (19)$$

$$g[h^0 \tilde{t}_1 \tilde{t}_1] = g_2 \left[\frac{\cos \alpha}{\sin \beta} \left(\frac{m_t A_t}{2m_W} \sin 2\theta_{\tilde{t}} - \frac{m_t^2}{m_W} \right) + \frac{\sin \alpha}{\sin \beta} \left(\frac{m_t \mu}{2m_W} \sin 2\theta_{\tilde{t}} \right) - \sin(\alpha + \beta) \left(\frac{m_Z(5 - 8c_w^2)}{6c_w} \cos^2 \theta_{\tilde{t}} - \frac{2m_Z s_w^2}{3c_w} \right) \right], \quad (20)$$

$$g[h^0 \tilde{t}_2 \tilde{t}_2] = g_2 \left[\frac{\cos \alpha}{\sin \beta} \left(-\frac{m_t A_t}{2m_W} \sin 2\theta_{\tilde{t}} - \frac{m_t^2}{m_W} \right) + \frac{\sin \alpha}{\sin \beta} \left(-\frac{m_t \mu}{2m_W} \sin 2\theta_{\tilde{t}} \right) - \sin(\alpha + \beta) \left(-\frac{m_Z(5 - 8c_w^2)}{6c_w} \cos^2 \theta_{\tilde{t}} + \frac{m_Z(1 - 4s_w^2)}{6c_w} \right) \right], \quad (21)$$

$$g[h^0 \tilde{b}_1 \tilde{b}_1] = g_2 \left[\frac{\sin \alpha}{\cos \beta} \left(-\frac{m_b A_b}{2m_W} \sin 2\theta_{\tilde{b}} + \frac{m_b^2}{m_W} \right) + \frac{\cos \alpha}{\cos \beta} \left(-\frac{m_b \mu}{2m_W} \sin 2\theta_{\tilde{b}} \right) - \sin(\alpha + \beta) \left(\frac{m_Z(4c_w^2 - 1)}{6c_w} \cos^2 \theta_{\tilde{b}} + \frac{m_Z s_w^2}{3c_w} \right) \right], \quad (22)$$

$$g[h^0 \tilde{b}_2 \tilde{b}_2] = g_2 \left[\frac{\sin \alpha}{\cos \beta} \left(\frac{m_b A_b}{2m_W} \sin 2\theta_{\tilde{b}} + \frac{m_b^2}{m_W} \right) + \frac{\cos \alpha}{\cos \beta} \left(\frac{m_b \mu}{2m_W} \sin 2\theta_{\tilde{b}} \right) - \sin(\alpha + \beta) \left(-\frac{m_Z(4c_w^2 - 1)}{6c_w} \cos^2 \theta_{\tilde{b}} + \frac{m_Z(1 + 2c_w^2)}{6c_w} \right) \right], \quad (23)$$

References

- [1] A. Djouadi *et al.*, hep-ph/0002258.
- [2] M. Carena *et al.*, hep-ph/0010338.
- [3] ATLAS-TDR, Volume II, CERN-LHCC-99-15.
- [4] H. M. Georgi, S. L. Glashow, M. E. Machacek and D. V. Nanopoulos, Phys. Rev. Lett. **40** (1978) 692; D. Graudenz, M. Spira and P. M. Zerwas, Phys. Rev. Lett. **70** (1993) 1372 ; S. Catani, D. de Florian and M. Grazzini, JHEP **05** (2001) 025 ; R. V. Harlander and W. B. Kilgore, Phys. Rev. Lett. **88** (2002) 201801 .
- [5] R. K. Ellis, I. Hinchliffe, M. Soldate and J. J. van der Bij, Nucl. Phys. B **297** (1988) 221.
- [6] U. Baur and E. W. Glover, Nucl. Phys. B **339** (1990) 38.
- [7] M. Chaichian, I. Liede, J. Lindfors and D. P. Roy, Phys. Lett. B **198** (1987) 416 [Erratum-ibid. B **205** (1987) 595].
- [8] S. Abdullin, M. Dubinin, V. Ilyin, D. Kovalenko, V. Savrin and N. Stepanov, Phys. Lett. B **431** (1998) 410 .
- [9] S. Dawson, A. Djouadi and M. Spira, Phys. Rev. Lett. **77** (1996) 16 .
- [10] O. Brein, W. Hollik and S. Kanemura, Phys. Rev. D **63** (2001) 095001 .
- [11] M. Carena, S. Heinemeyer, C. E. Wagner and G. Weiglein, hep-ph/9912223.
- [12] M. Carena, H. E. Haber, H. E. Logan and S. Mrenna, Phys. Rev. D **65** (2002) 055005 [Erratum-ibid. D **65** (2002) 099902] .
- [13] S. Heinemeyer, W. Hollik and G. Weiglein, Eur. Phys. J. C **9** (1999) 343; Eur. Phys. J. C **16** (2000) 139; hep-ph/0002213 .
- [14] A. Djouadi, P. Gambino, S. Heinemeyer, W. Hollik, C. Jünger and G. Weiglein, Phys. Rev. D **57** (1998) 4179.
- [15] [LEP Higgs Working Group Collaboration], hep-ex/0107030.
- [16] K. Hagiwara *et al.* [Particle Data Group Collaboration], Phys. Rev. D **66** (2002) 010001.
- [17] R. Brock *et al.* [CTEQ Collaboration], *Handbook of perturbative QCD: Version 1.0*, Rev. Mod. Phys. **67** (1995) 157.

- [18] D. Dicus, T. Stelzer, Z. Sullivan and S. Willenbrock, Phys. Rev. D **59** (1999) 094016.
- [19] A. D. Martin, R. G. Roberts, W. J. Stirling and R. S. Thorne, Eur. Phys. J. C **4** (1998) 463.
- [20] J. Küblbeck, M. Böhm and A. Denner, Comput. Phys. Commun. **60** (1990) 165; H. Eck, Ph.D. thesis, University of Würzburg (1995); T. Hahn and M. Perez-Victoria, Comput. Phys. Commun. **118** (1999) 153; T. Hahn, Comput. Phys. Commun. **140** (2001) 418, T. Hahn and C. Schappacher, Comput. Phys. Commun. **143** (2002) 54.

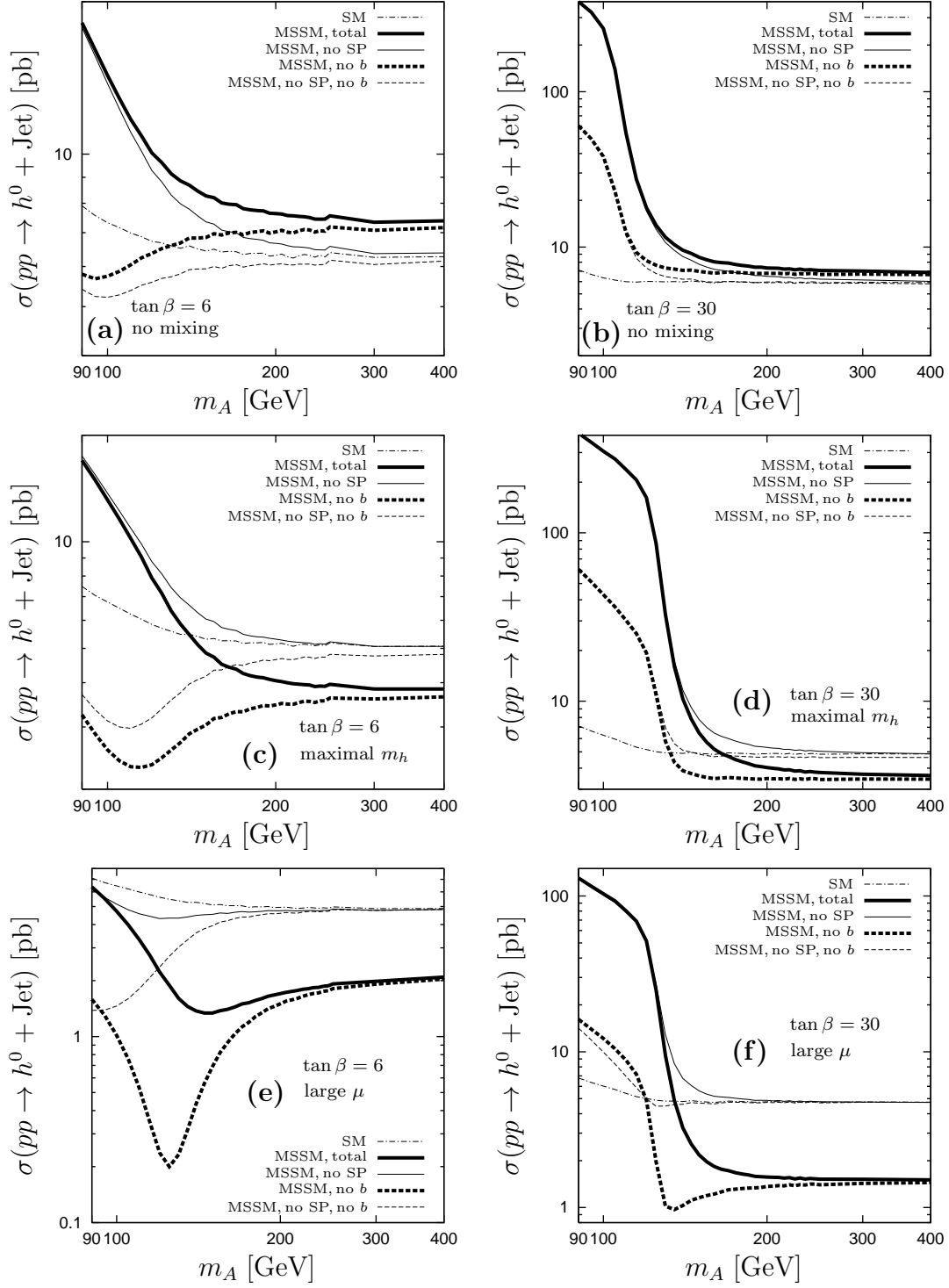


Figure 6: Hadronic cross section for the process $pp \rightarrow h^0 + \text{jet}$ as a function of m_A . The results of the three benchmark scenarios with $M_{\text{SUSY}} = 400$ GeV are displayed for $\tan\beta = 6$ and 30.

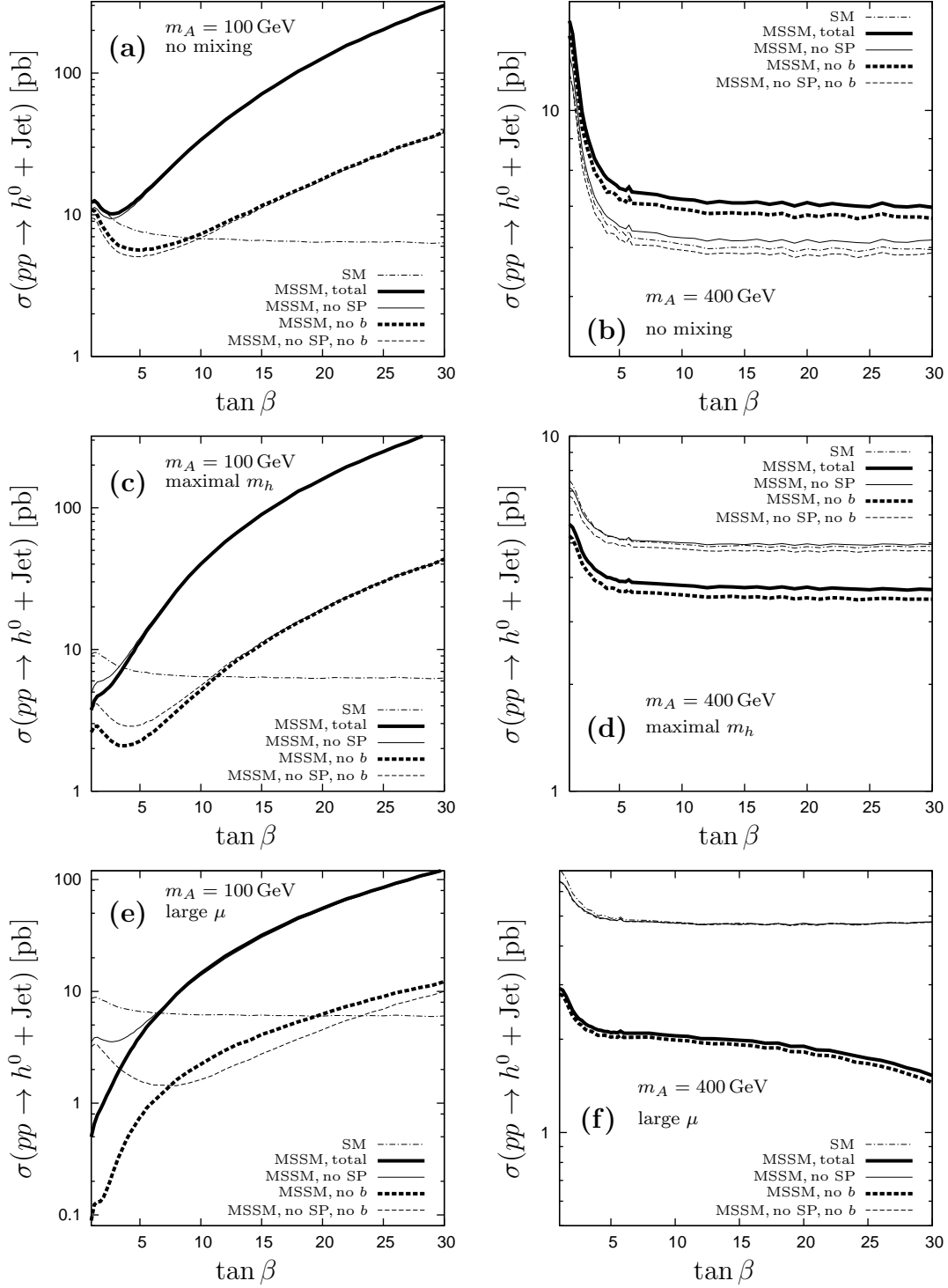


Figure 7: Hadronic cross section for the process $pp \rightarrow h^0 + \text{jet}$ as a function of $\tan \beta$. The results of the three benchmark scenarios with $M_{\text{SUSY}} = 400$ GeV are displayed for $m_A = 100$ GeV and 400 GeV.

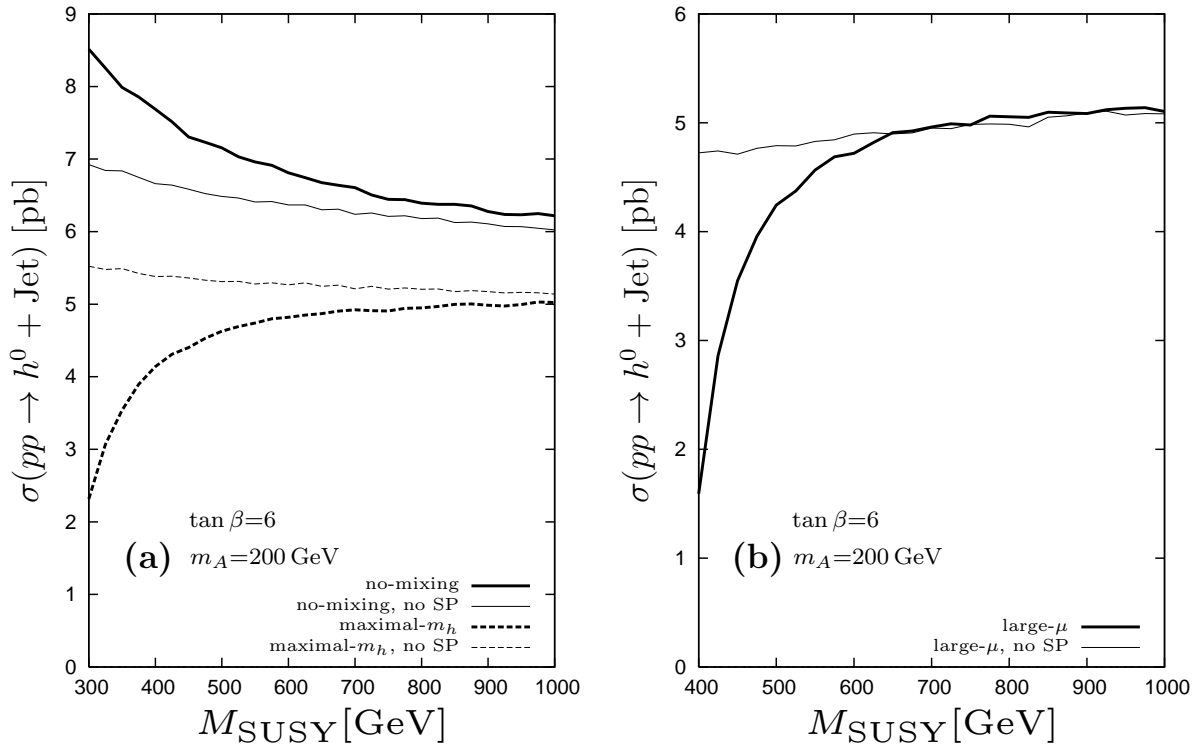


Figure 8: Hadronic cross section for Higgs plus jet production versus M_{SUSY} . $m_A = 200$ GeV and $\tan\beta = 6$. The cross section prediction is shown for the no-mixing (solid lines) and maximal- m_h scenario (dashed lines) in panel (a) and for the large- μ scenario in panel (b). Thick lines indicate the full result, while thin lines are obtained by leaving out all Feynman graphs with superpartner loops in the calculation.

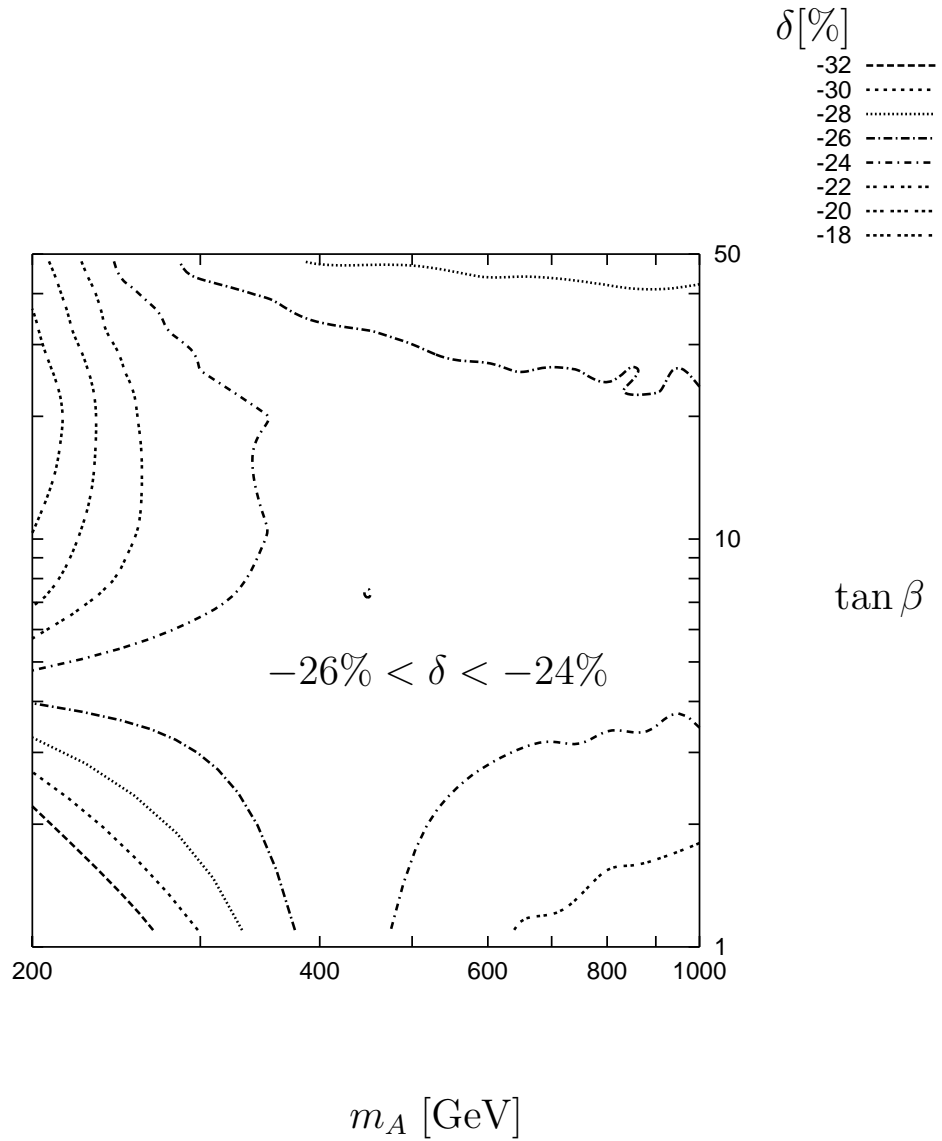


Figure 9: Relative difference δ between the MSSM result and the corresponding SM result (with identical Higgs mass) for the hadronic cross section for Higgs plus jet production. The dependence of $\delta = (\sigma^{\text{MSSM}} - \sigma^{\text{SM}})/\sigma^{\text{SM}}$ on m_A and $\tan \beta$ is indicated by contour lines. Here the maximal- m_h scenario with $M_{\text{SUSY}} = 400$ GeV is chosen.